Topological Magnon Band Crossing in $Y_2Ir_2O_7$

Thi Huyen Nguyen,[1,2,*] Jaeseok Son,[1,2,*] Soyeun Kim,[1,2,†] Hwanbeom Cho,[1,2,‡] Choong H. Kim,[1,2] Y. P. Wang,[3] Kenneth S. Burch,[3] In-Sang Yang,[4] Jaehong Jeong,[1,2] Je-Geun Park,[1,2,5] S. J. Moon,[6,§] and T. W. Noh[1,2,‖]

[1]*Center for Correlated Electron Systems, Institute for Basic Science (IBS), Seoul 08826, Republic of Korea*
[2]*Department of Physics and Astronomy, Seoul National University, Seoul 08826, Republic of Korea*
[3]*Physics Department, Boston College, Boston, Massachusetts 02467, USA*
[4]*Department of Physics, Ewha Womans University, Seoul 03760, Republic of Korea*
[5]*Center for Quantum Materials, Seoul National University, Seoul 08826, Republic of Korea*
[6]*Department of Physics, Hanyang University, Seoul 04763, Republic of Korea*

(Received 8 June 2021; accepted 22 November 2021; published 23 December 2021)

Topological magnonic materials have attracted much interest because of the potential for dissipationless spintronic applications. Pyrochlore iridates are theoretically regarded as good candidates for designing topological magnon bands. However, experimental identification of topological magnon bands in pyrochlore iridates remains elusive. We explored this possibility in $Y_2Ir_2O_7$ using Raman spectroscopy to measure both the single-magnon excitations and anomalous phonon shifts. From the single-magnon energies and tight-binding model calculations concerning the phonons, we determined the key parameters in the spin Hamiltonian. These confirm that $Y_2Ir_2O_7$ hosts a nontrivial magnon band topology distinct from other pyrochlore iridate compounds. Our work demonstrates that pyrochlore iridates constitute a system in which the magnon band topology can be tailored and that Raman spectroscopy is a powerful technique to explore magnon band topology.

DOI: 10.1103/PhysRevLett.127.267203

Topological magnon band (MB) with linear band crossing protected by symmetries can have nonzero Berry curvature which produces the thermal Hall effect [1,2]. Because of the charge-free character, topological magnons can enable dissipationless transport in insulating magnets [1,3]. Thus, topological magnonic materials are of fundamental interest and highly desired for developing high-efficiency and low-cost spintronic devices [4,5]. Topological MB crossing, which can form a Weyl point, has been proposed to appear in limited systems of pyrochlore ferromagnets or noncentrosymmetric antiferromagnets [6,7]. While topological MB crossing was observed in a three-dimensional collinear antiferromagnet [5,8], experimental evidence of topological MB has rarely been reported in other materials.

The pyrochlore iridates $R_2Ir_2O_7$ (R = Y, rare-earth ions) offer an excellent opportunity to pursue the creation of topological MB. By manipulating small structural details with R, the magnetic interactions can be fine-tuned to create the desired topological phase. Using linear spin-wave theory (LSWT) calculations, Hwang *et al.* suggested a topological MB phase diagram of $R_2Ir_2O_7$ [9]. Their calculations showed that the four lowest-lying MBs have single and triple degeneracies at the Γ point. As shown in Fig. 1(a), when the triply degenerate state is located at lower energy, the MBs cross at a $\boldsymbol{k}$ point along the ΓX lines which is protected by $\bar{T}_d$ symmetry; we will call this a crossing MB (c-MB) phase. Conversely, when the triply

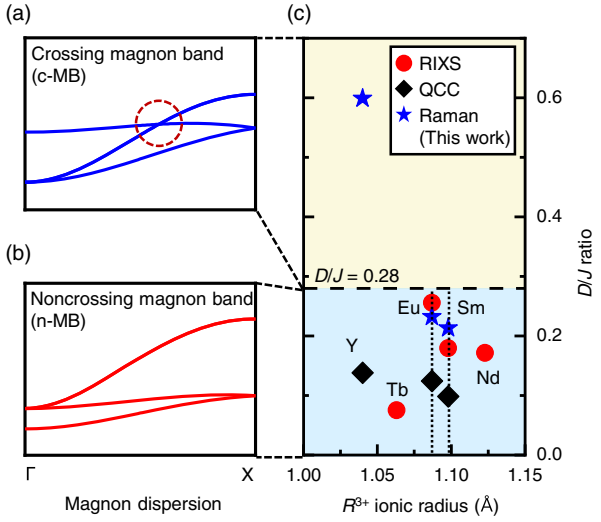

FIG. 1. (a)–(b) Dispersions for crossing magnon band (c-MB) and noncrossing magnon band (n-MB). (c) Magnon band topology phase diagram for some pyrochlore iridates $R_2Ir_2O_7$ (R = Y, Tb, Eu, Sm, and Nd). We note that $D/J = 0.28$ in Ref. [9] is the boundary between the c-MB and n-MB topology, where the Dzyaloshinskii-Moriya interaction and the Heisenberg interaction are denoted by D and J, respectively. Red dots are D/J values obtained from resonant inelastic x-ray scattering experiments and black diamonds are parameters from quantum chemistry calculations (QCC). The parameters used for this phase diagram are listed in the Supplemental Material [10]. Our Raman data (blue star) suggest $Y_2Ir_2O_7$ is in the c-MB phase, contrary to the result of the QCC.

degenerate state is located at higher energy, the MBs cannot make any crossing [Fig. 1(b)]; we will call this the noncrossing MB (n-MB) phase.

Hwang *et al.* also found that the ratio between Dzyaloshinskii-Moriya interaction (D) and Heisenberg interaction (J) plays a key role in controlling MB topology [9]. When $D/J < 0.28$, $R_2Ir_2O_7$ will have n-MB. In contrast, when $D/J > 0.28$, $R_2Ir_2O_7$ will have c-MB [10]. The distinct MB topology can lead to differences in thermal Hall effects [9] and offers a new means to tune a system through a topological phase transition.

To search for this intriguing topological phase transition, accurate values of D/J in real $R_2Ir_2O_7$ systems must be determined. Thus far, it has been difficult to obtain accurate J and D values of $R_2Ir_2O_7$. Because Ir^{4+} ions strongly absorb neutrons, inelastic neutron scattering cannot be applied to pyrochlore iridates. For resonant inelastic x-ray scattering (RIXS) [23–25], the resolution of this experimental technique is 25–28 meV, which is much larger than the predicted energy difference of about 4 meV between the nondegenerate and triply degenerate MBs at the Γ point in $R_2Ir_2O_7$ [9,23]. Theoretical quantum chemistry calculations (QCC) have been widely applied, but their calculational results are highly dependent on the Ir—O—Ir bond-angle (θ) [26]. We note that all reported D/J values for $R_2Ir_2O_7$ are located at the n-MB phase [Fig. 1(c)], suggesting the absence of the topological phase transition in $R_2Ir_2O_7$. In addition, the D/J values of each technique do not show systematic evolution with the variation in radius of rare-earth ions.

Here, we describe the use of Raman spectroscopy to study magnetic interactions of $Y_2Ir_2O_7$ which shows all-in-all-out (AIAO) antiferromagnetic (AFM) order below $T_N = 170$ K. Upon cooling into the AIAO state, two magnetic excitation peaks emerge at 231 cm^{-1} (28.6 meV) and 277 cm^{-1} (34.4 meV). In combination with tight-binding model calculation, we found that these Raman peaks originate from the single-magnon scattering (1MS), rather than the two-magnon scattering (2MS) that commonly appears in most magnetic materials [26]. We also observed an abrupt phonon peak shift of the A_{1g} mode ~2.3 cm^{-1} below T_N, implying spin-phonon coupling (SPC). Analysis of SPC and single-magnon excitations allowed us to accurately determine the D/J value: $D/J \sim 0.60$ ($J = 15.1$ and $D = 9.0$ meV) for $Y_2Ir_2O_7$. Our results suggest that $Y_2Ir_2O_7$ is the first candidate for c-MB topology among noncollinear AFM $R_2Ir_2O_7$ [Fig. 1(c)]. The results further reveal that the pyrochlore iridate is a unique system where the magnon band topology can be readily tuned, which is a challenging task in electronic counterparts [27].

Figure 2(a) shows the Raman spectrum of $Y_2Ir_2O_7$ at 10 K. Six Raman-active phonon modes were observed, consistent with factor group analysis for the Fd-3m space group [28,29]. We performed density functional theory (DFT) calculations to assign the symmetry of phonon

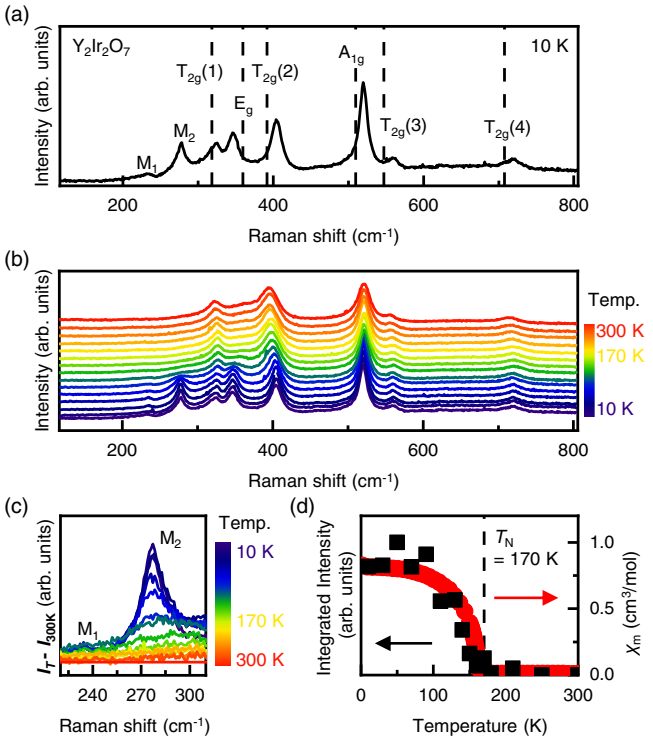

FIG. 2. (a) Raman spectra of polycrystalline $Y_2Ir_2O_7$ at 10 K. The frequencies of the six Raman-active phonons are calculated using density functional theory calculations (dashed lines). M_1 and M_2 correspond to magnetic excitations. (b) Temperature (T)-dependent Raman spectra of $Y_2Ir_2O_7$. (c) T-dependent Raman spectra of magnetic excitation peaks in $Y_2Ir_2O_7$. For clarity, each spectral intensity I_T at various T is subtracted by the intensity of reference spectrum $I_{300\,K}$ at 300 K. (d) T dependence of the integrated intensity of the magnetic excitations in the range of 208 and 314 cm^{-1} (black squares) and magnetic susceptibility χ_m measured at $H = 0.1$ T after zero-field cooling (red circles). For integration, we subtracted the 300 K spectra from the spectra at the other temperatures and integrated them in the energy range between 208 and 314 cm^{-1}.

modes [10]. The calculated and experimental phonon frequencies showed good agreement, allowing assignment of the observed phonon modes [10]. The Raman spectra of $Y_2Ir_2O_7$ showed two peaks below 300 cm^{-1} marked as M_1 and M_2, which could not be assigned as phonon modes. These well-resolved sharp peaks were located at 231 cm^{-1} (28.6 meV) and 277 cm^{-1} (34.4 meV) for M_1 and M_2, respectively. By changing the laser source from 532 to 671 nm, we confirmed that the M peaks originated from Raman excitation, rather than photoluminescence [10]. The AIAO magnetic ordering protects the cubic lattice symmetry of $R_2Ir_2O_7$ [30], suggesting that the M peaks are not associated with zone-folded phonon in the AFM state. In addition, previous x-ray and neutron diffraction studies of $R_2Ir_2O_7$ found no structural phase transitions [31,32], confirming that the M peaks are irrelevant to lattice distortions.

To further investigate the nature of the M peaks, we studied the temperature (T) dependence of the Raman spectra of $Y_2Ir_2O_7$ [Fig. 2(b)]. We found that the M peaks are visible only in the AFM state. The evolution of the M peaks is more clearly visible in the difference spectra I_T-$I_{300\ K}$ shown in Fig. 2(c). As T increases from 10 to 150 K, the M peaks are significantly suppressed and become indistinguishable above T_N. Figure 2(d) shows the T-dependent integrated intensities from the spectra I_T-$I_{300\ K}$ of the M peaks (black squares) and magnetic susceptibilities (red circles). The integrated intensities of both peaks reveal anomalies at T_N, suggesting a magnetic origin of the M peaks.

The magnon dispersion of the AIAO magnet has been studied extensively from a theoretical perspective [9,33]. The fourfold-degenerate magnon dispersion in $R_2Ir_2O_7$ is strongly affected by the Dzyaloshinskii-Moriya interaction, which exhibits a gap at the Γ point. Figure 3(a) summarizes the information related to MB for $Sm_2Ir_2O_7$, $Eu_2Ir_2O_7$, and $Y_2Ir_2O_7$. The red-colored regions indicate the bandwidth of MB from RIXS studies [23–25]. They indicate that the MB gap energies of $Sm_2Ir_2O_7$ and $Eu_2Ir_2O_7$ are ∼25 and ∼28 meV, respectively. To the best of our knowledge, no experimental information concerning MB is available for $Y_2Ir_2O_7$ [31,34]. The energies of magnetic excitations of $Sm_2Ir_2O_7$ and $Eu_2Ir_2O_7$ from our Raman data are indicated by black solid lines in Fig. 3(a) [10]. Previous Raman studies of $Sm_2Ir_2O_7$ and $Eu_2Ir_2O_7$ also reported the magnetic excitation peaks at nearly the same energies [10,28,29]. The energies of the magnetic excitations of $Sm_2Ir_2O_7$ and $Eu_2Ir_2O_7$ are found to be close to their magnon dispersion gap energies [10,23–25]. These similarities suggest that the Raman peaks of $Sm_2Ir_2O_7$ and $Eu_2Ir_2O_7$ may correspond to 1MS.

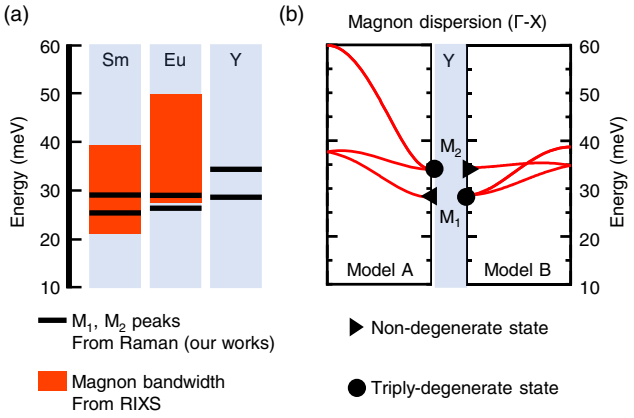

FIG. 3. (a) Magnetic excitation energy diagram for $R_2Ir_2O_7$. Black lines indicate the energies of M_1 and M_2 from our Raman experiments (for $Sm_2Ir_2O_7$ and $Eu_2Ir_2O_7$, see Supplemental Material [10]). The magnon bandwidths obtained from the RIXS measurements are shaded in red [23–25]. (b) Magnon dispersion of $Y_2Ir_2O_7$ based on the linear spin-wave theory calculations with two Hamiltonian models in this work: Model A, where $J = 37.6$, $D = 7.0$ meV and nondegenerate (triangles) $\equiv M_1$, triply degenerate (circles) $\equiv M_2$ energy; and model B, where for $J = 15.1$, $D = 9.0$ meV with triply degenerate $= M_1$, nondegenerate $= M_2$ energy.

Similarly, we attribute the M peaks in the Raman spectra of $Y_2Ir_2O_7$ to 1MS. Note that, in magnetic materials, Raman spectra usually show 2MS peaks, which are generally much stronger than 1MS peaks [35]. However, as shown in Figs. 3(a)–3(b), the resonance energies of the M peaks of $Y_2Ir_2O_7$ are close to the gap energies in the magnon dispersion of $Sm_2Ir_2O_7$ and $Eu_2Ir_2O_7$ as well as to the energies of 1MS in their Raman spectra [23–25,28,29]. In addition, the M peaks are much sharper (∼17 cm^{-1}) than are the 2MS peaks (250–400 cm^{-1} for $R_2Ir_2O_7$) [20,36]. Symmetry (Raman tensors) analysis of $R_2Ir_2O_7$ based on the pseudospin $J_{\rm eff} = 1/2$ configuration further supports the conclusion that the M peaks are attributable to 1MS [10,37].

In general, the magnetic Hamiltonian for AIAO pyrochlore iridates can be written as

$$H_{\rm spin} = \sum_{ij}^{nn} [JS_i \cdot S_j + D_{ij}(S_i \times S_j) + S_i \cdot \mathbb{A}_{ij} \cdot S_j], \quad (1)$$

where J and D are the Heisenberg and Dzyaloshinskii-Moriya interactions, respectively. Magnetic pyrochlore materials can also have anisotropic exchange interaction $\mathbb{A}$. Because $\mathbb{A}$ has values in an order of magnitude smaller than J and D in $R_2Ir_2O_7$ [10], we will focus on the J and D values in this Letter. Using Eq. (1), Hwang *et al.* derived the MB dispersions of $R_2Ir_2O_7$ [9]. At the Γ point the MB has triply and singly degenerate states with E_t and E_s, respectively. E_t and E_s can be expressed analytically in terms of J and D:

$$E_t = 2S\sqrt{\frac{(8\sqrt{2}(J+2\mathbb{A}) + 14(D - \frac{3\sqrt{2}}{4}\mathbb{A}))(D - \frac{3\sqrt{2}}{4}\mathbb{A})}{3}}, \quad (2)$$

$$E_s = 2S \cdot 3\sqrt{2}\left(D - \frac{3\sqrt{2}}{4}\mathbb{A}\right). \quad (3)$$

If the M peaks originate from the 1MS Raman process, they should correspond to E_s and/or E_t excitations. However, there are two possible scenarios for 1MS: E_s is smaller or larger than E_t. We considered both cases: Model A ($M_1 \equiv E_s, M_2 \equiv E_t$) and model B ($M_1 \equiv E_t$, $M_2 \equiv E_s$). Using Eqs. (2) and (3), we determined that $J = 37.6$ and $D = 7.0$ meV for model A (and $J = 15.1$ and $D = 9.0$ meV for model B). The magnon dispersions for models A and B are plotted in Fig. 3(b). The two models show very different MB dispersions: Model A indicates an n-MB phase and model B indicates a c-MB phase. The D/J

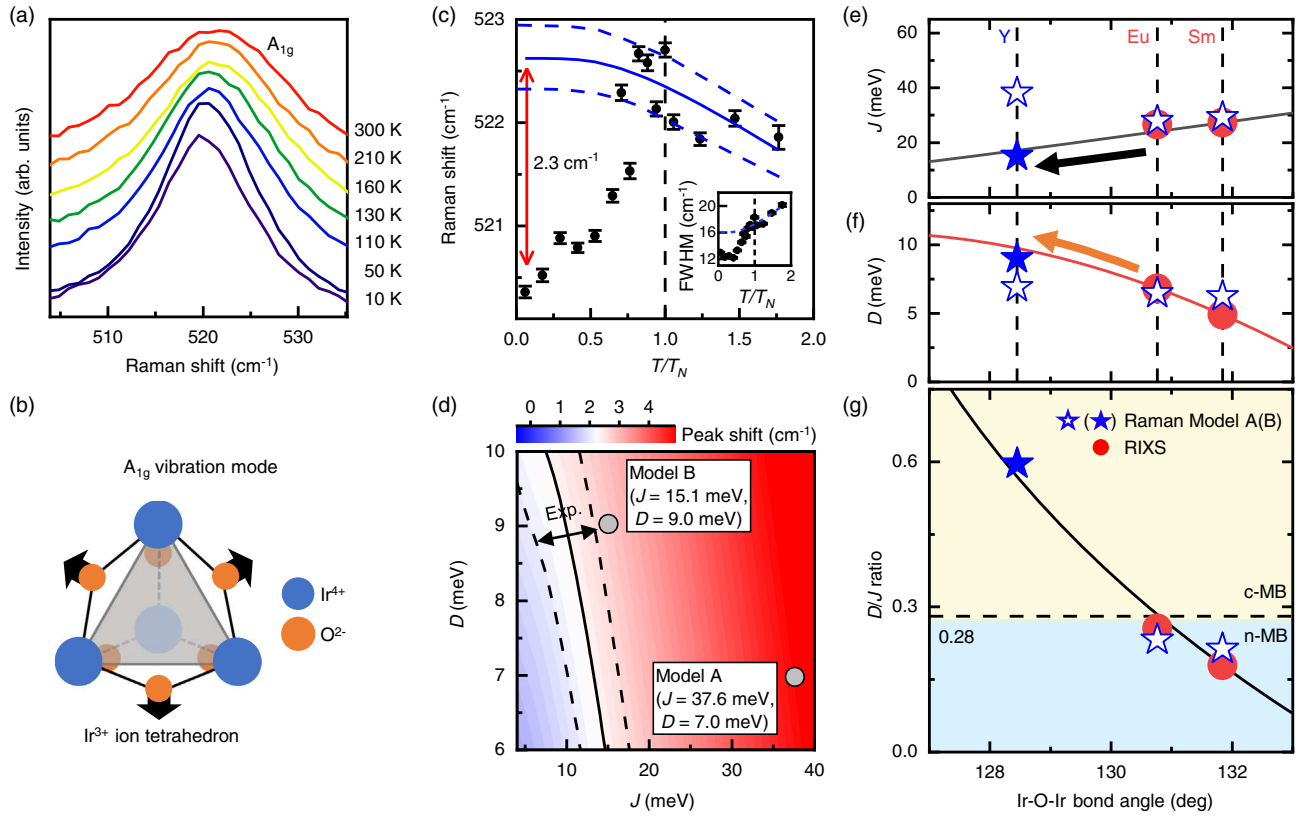

FIG. 4. (a) T evolution of the A_{1g} phonon. (b) Atomic displacement of the A_{1g} phonon of $Y_2Ir_2O_7$. (c) T dependence of the phonon shift (black circles) and the full width at half maximum (FWHM, black squares in the inset) of the A_{1g} phonon obtained by Lorentzian fitting. Blue solid and dashed lines are the anharmonic fitting curves for the T dependence of the phonon shift and linewidth. Thermal fluctuations of the peak shift around T_N indicate that the fitting curve for the peak shift in (c) is not unique, leading to a shift of the A_{1g} phonon of approximately $\Delta\omega = 2.3 \pm 0.3$ cm^{-1}. (d) Contour map of the phonon shift calculated for J and D values. The peak shift is indicated by color coding. Solid and dashed lines indicate the experimental values of the peak shift and error bars: $\Delta\omega = 2.3 \pm 0.3$ cm^{-1}. Gray circles represent the calculated peak shifts corresponding to the J and D parameters of models A and B. (e)–(g) Ir—O—Ir bond-angle (θ) dependence of J and D obtained from tight-binding calculations on $R_2Ir_2O_7$ (R: Sm, Eu, Y). The calculated curves of $J(\theta)$ and $D(\theta)$ agree with the J and D values in model B for $Y_2Ir_2O_7$ but differ markedly from the J and D values in model A.

values of models A and B are approximately 0.18 and 0.60, respectively.

To determine which of these models is correct, we investigated the T dependence of Raman-active phonon peaks. Our earlier infrared (IR) spectroscopy study of $Y_2Ir_2O_7$ indicated that the three phonon modes show anomalous softening below T_N, attributable to SPC [38]. As shown in Fig. 4(a), our Raman spectra of the A_{1g} mode show similar phonon softening below T_N [39]. The atomic displacement of the A_{1g} mode is depicted in Fig. 4(b). To obtain quantitative information, we fit the A_{1g} mode by using the Lorentzian line shape [10]. The T evolution of the Raman shift is shown in Fig. 4(c). Above T_N, the A_{1g} phonon frequency follows a monotonic blueshift [blue solid lines in Fig. 4(c)] with decreasing T due to the anharmonic decay process, which can be described by $\omega_T = \omega_0 + A(1 + \{2/[\exp(h\omega_0/2k_BT) - 1]\})$ where ω_0 and A are constants [40]. Below T_N, in contrast, the frequency of the A_{1g} mode significantly deviates from the thermal behavior and softens with decreasing T. Such T evolution implies strong SPC. The full width at half maximum of the A_{1g} mode also exhibits a kink at T_N, as shown in the inset of Fig. 4(c). We define the peak shift $\Delta\omega = \omega_0 - \omega_{10\,\mathrm{K}}$, where ω_0 is the constant obtained during the fitting process; experimental $\Delta\omega$ for the A_{1g} mode is $\sim 2.3 \pm 0.3$ cm^{-1}.

To extract the J and D values from the anomalous phonon softening, we calculated the J- and D-dependent $\Delta\omega$ using tight-binding model calculations [38]. Our calculations predict that the Dzyaloshinskii-Moriya interaction is the main contributor to phonon softening below T_N [10], consistent with the conclusion from the T dependence of IR-active phonons of $Y_2Ir_2O_7$ [38]. Figure 4(d) shows a contour plot of the calculated peak shift $\Delta\omega$ of the A_{1g} phonon mode for various J and D values. The solid line and two dashed lines display the J

and D values, which can produce the peak shift with error bars: $\Delta\omega = 2.3 \pm 0.3$ cm^{-1}. The gray circles indicate the J and D values obtained from Eqs. (2) and (3) for models A and B. Importantly, only model B (i.e., $J = 15.1$ and $D = 9.0$ meV) can explain the experimental phonon shift. The calculated $\Delta\omega$ values from models A and B are approximately 5.0 and 2.6 cm^{-1}, respectively. Therefore, we concluded that the MB dispersion of $Y_2Ir_2O_7$ can be described by model B with c-MB topology.

To further confirm that model B correctly describes the magnon dispersion, we performed tight-binding model calculations on the Ir—O—Ir angle (θ) dependence of J and D in $R_2Ir_2O_7$. Electron hopping between the nearest neighbor Ir ions contributes to J and D. In $R_2Ir_2O_7$, the hopping integral depends on θ, thus affecting the J and D values. We used the θ values of the $R_2Ir_2O_7$ compounds from the previous x-ray diffraction (XRD) and neutron diffraction studies [31,41]. Details of the θ dependence of J and D are provided in Ref. [38].

In Figs. 4(e)–4(f), we compare the calculational results for $Y_2Ir_2O_7$, $Eu_2Ir_2O_7$, and $Sm_2Ir_2O_7$ with those from previous RIXS studies [23–25]. The values of θ, J, and D are summarized in the Supplemental Material [10]. The empty and solid stars correspond to J and D values for models A and B, respectively. The calculations of the θ dependence of J and D indicate that model B ($J = 15.1$ and $D = 9.0$ meV) can appropriately represent the magnetic excitations in $Y_2Ir_2O_7$.

The D/J curve generated from the θ-dependent J and D is shown in Fig. 4(g). The D/J curve shows a systematic dependence on θ: as θ decreases, D/J increases. The trigonal distortion of the oxygen octahedra in $R_2Ir_2O_7$ is larger at smaller θ, demonstrating that the trigonal distortion enhances the Dzyaloshinskii-Moriya interactions between the Ir^{4+} ion network. More importantly, the D/J curve suggests that a topology change in MB can occur in $R_2Ir_2O_7$ [9]. Recall that $D/J = 0.28$ is a boundary separating n-MB (light blue area) and c-MB (yellow area). The $D/J = 0.60$ of $Y_2Ir_2O_7$ in this work indicates that $Y_2Ir_2O_7$ is the first material that could have c-MB among pyrochlore iridates. This finding also demonstrates that the topological phase of the MB can be easily tuned in $R_2Ir_2O_7$, which has been demanding in electronic materials [42,43]. Further investigations are required concerning MB and related physical properties, such as thermal Hall conductivities.

Through a combined Raman spectroscopy and tight-binding model calculation study, we showed that $Y_2Ir_2O_7$ hosts the crossing magnon band topology for the first time. The analyses on the resonance energies of the single magnon excitations and the anomalous phonon softening in the antiferromagnetic phase led to a unique determination of the magnetic interaction parameters of $R_2Ir_2O_7$. The values of the magnetic interaction parameters from our analyses indicate that $Y_2Ir_2O_7$ has the crossing magnon band and $Sm_2Ir_2O_7/Eu_2Ir_2O_7$ shows noncrossing magnon bands. The distinct magnon band topologies are expected to manifest themselves in the thermal Hall effect. It is worth performing magnon thermal Hall measurements to confirm the rich phases of the nontrivially topological properties $R_2Ir_2O_7$. Our result indicates that the pyrochlore iridates $R_2Ir_2O_7$ is a unique system where the magnon band topology can be tuned, which has been challenging in topological electronic systems. Our study also suggests that Raman spectroscopy is a simple and powerful tool to investigate magnon excitations and spin Hamiltonian of the AIAO $5d$ pyrochlore iridate $R_2Ir_2O_7$.

This work was supported by the Research Center Program of IBS (Institute for Basic Science) in Korea (IBS-R009-D1). Y. Wang is grateful for the support of the Office of Naval Research under Grant No. N00014-20-1-2308, and K. S. Burch acknowledges support from the Air Force Office of Scientific Research under Grant No. FA9550-20-1-0282. I.-S. Y. was supported by the National Research Foundation of Korea (NRF) grant funded by the Korean government (MSIT) (2017R1A2B2009309). J.-G. P. was supported by the Leading Researcher Program of the National Research Foundation of Korea (Grant No. 2020R1A3B2079375). S. J. M. was supported by the National Research Foundation grant of Korea (NRF) funded by the Korean government (MSIT) (2019R1A2C1084237).

T. H. N. and J. S. contributed equally to this work. T. H. N., J. S., S. Y. K., Y. W., K. S. B., and I.-S. Y. performed and assisted in the Raman experiments. H. B. C. and J.-G. P. prepared the sample. T. H. N., J. S., and J. H. J. analyzed the experimental data. C. H. K. performed the DFT calculations. T. H. N., J. S., S. J. M., T. W. N. wrote the paper with input from all co-authors.

*These authors contributed equally to this work.
†Present address: Department of Physics, University of Illinois at Urbana Champaign, Urbana, Illinois 61801, USA.
‡Present address: Clarendon Laboratory, University of Oxford, Parks Road, Oxford OX1 3PU, United Kingdom.
§soonjmoon@hanyang.ac.kr
‖twnoh@snu.ac.kr

[1] Y. Onose, T. Ideue, H. Katsura, Y. Shiomi, N. Nagaosa, and Y. Tokura, Science **329**, 297 (2010).
[2] J. Romhányi, K. Penc, and R. Ganesh, Nat. Commun. **6**, 6805 (2015).
[3] L. Zhang, J. Ren, J.-S. Wang, and B. Li, Phys. Rev. B **87**, 144101 (2013).
[4] A. V. Chumak, V. I. Vasyuchka, A. A. Serga, and B. Hillebrands, Nat. Phys. **11**, 453 (2015).
[5] W. Yao, C. Li, L. Wang, S. Xue, Y. Dan, K. Iida, K. Kamazawa, K. Li, C. Fang, and Y. Li, Nat. Phys. **14**, 1011 (2018).
[6] F. Y. Li, Y. D. Li, Y. B. Kim, L. Balents, Y. Yu, and G. Chen, Nat. Commun. **7**, 12691 (2016).

[7] A. Mook, J. Henk, and I. Mertig, Phys. Rev. Lett. **117**, 157204 (2016).

[8] K. Li, C. Li, J. Hu, Y. Li, and C. Fang, Phys. Rev. Lett. **119**, 247202 (2017).

[9] K. Hwang, N. Trivedi, and M. Randeria, Phys. Rev. Lett. **125**, 047203 (2020).

[10] See Supplemental Material at http://link.aps.org/supplemental/10.1103/PhysRevLett.127.267203 for details regarding anisotropic exchange interactions, magnetic interaction parameters, and structure information of $R_2Ir_2O_7$; comparison of calculated and experimental phonon frequencies, laser dependence of the M_1 and M_2 peaks, Raman spectra of other pyrochlore iridates, magnetic point group analysis for AIAO pyrochlore iridate, single-magnon scattering mechanism in pseudospin configuration, spin-phonon coupling driven by Dzyaloshinskii-Moriya interaction, and the asymmetric Fano line shape of the A_{1g} mode, which includes Refs. [11–22].

[11] H. Guo, C. Ritter, and A. C. Komarek, Phys. Rev. B **94**, 161102(R) (2016).

[12] E. Lefrancois, V. Simonet, R. Ballou, E. Lhotel, A. Hadj-Azzem, S. Kodjikian, P. Lejay, P. Manuel, D. Khalyavin, and L. C. Chapon, Phys. Rev. Lett. **114**, 247202 (2015).

[13] G. Kresse and J. Hafner, Phys. Rev. B **48**, 13115 (1993).

[14] S. M. Disseler, Phys. Rev. B **89**, 140413(R) (2014).

[15] Y. Tian *et al.*, Rev. Sci. Instrum. **87**, 043105 (2016).

[16] S. Singh, S. Saha, S. K. Dhar, R. Suryanarayanan, A. K. Sood, and A. Revcolevschi, Phys. Rev. B **77**, 054408 (2008).

[17] L. Benfatto and M. B. S. Neto Phys. Rev. B **74**, 024415 (2006).

[18] R. Birss, in *Symmetry and Magnetism*, Science Education and Future Human Needs Series (North-Holland Publishing Company, Amsterdam, 1966).

[19] R. J. Elliott and R. Loudon, Phys. Lett. **3**, 189 (1963).

[20] A. P. Cracknell, J. Phys. C **2**, 500 (1969).

[21] U. Fano, Phys. Rev. **124**, 1866 (1961).

[22] T. M. H. Nguyen *et al.*, Nat. Commun. **8**, 251 (2017).

[23] C. Donnerer, M. C. Rahn, M. M. Sala, J. G. Vale, D. Pincini, J. Strempfer, M. Krisch, D. Prabhakaran, A. T. Boothroyd, and D. F. McMorrow, Phys. Rev. Lett. **117**, 037201 (2016).

[24] C. Donnerer, Ph. D. thesis, University College London, 2017.

[25] S. H. Chun, B. Yuan, D. Casa, J. Kim, C. Y. Kim, Z. Tian, Y. Qiu, S. Nakatsuji, and Y. J. Kim, Phys. Rev. Lett. **120**, 177203 (2018).

[26] R. Yadav, M. Pereiro, N. A. Bogdanov, S. Nishimoto, A. Bergman, O. Eriksson, J. van den Brink, and L. Hozoi, Phys. Rev. Mater. **2**, 074408 (2018).

[27] T. I. Andersen *et al.*, Nat. Mater. **20**, 480 (2021).

[28] K. Ueda, R. Kaneko, A. Subedi, M. Minola, B. J. Kim, J. Fujioka, Y. Tokura, and B. Keimer, Phys. Rev. B **100**, 115157 (2019).

[29] T. Hasegawa, N. Ogita, K. Matsuhira, S. Takagi, M. Wakeshima, Y. Hinatsu, and M. Udagawa, J. Phys. Conf. Ser. **200**, 012054 (2010).

[30] Z. Hiroi, J. Yamaura, T. Hirose, I. Nagashima, and Y. Okamoto, APL Mater. **3**, 041501 (2015).

[31] M. C. Shapiro, S. C. Riggs, M. B. Stone, C. R. de la Cruz, S. Chi, A. A. Podlesnyak, and I. R. Fisher, Phys. Rev. B **85**, 214434 (2012).

[32] J. P. Clancy *et al.*, Phys. Rev. B **94**, 024408 (2016).

[33] E. K.-H. Lee, S. Bhattacharjee, and Y. B. Kim, Phys. Rev. B **87**, 214416 (2013).

[34] L. Hozoi *et al.*, Phys. Rev. B **89**, 115111 (2014).

[35] P. A. Fleury and R. Loudon, Phys. Rev. **166**, 514 (1968).

[36] S.-M. Souliou, J. Chaloupka, G. Khaliullin, G. Ryu, A. Jain, B. J. Kim, M. Le Tacon, and B. Keimer, Phys. Rev. Lett. **119**, 067201 (2017).

[37] X. Wan, A. M. Turner, A. Vishwanath, and S. Y. Savrasov, Phys. Rev. B **83**, 205101 (2011).

[38] J. Son, B. C. Park, C. H. Kim, H. Cho, S. Y. Kim, L. J. Sandilands, C. Sohn, J.-G. Park, S. J. Moon, and T. W. Noh, npj Quantum Mater. **4**, 17 (2019).

[39] The E_g phonon mode at about 346.3 cm^{-1} seems to show a hardening and abrupt intensity reduction, as the temperature increases across T_N. However, since the E_g mode overlaps strongly with two other T_{2g} phonons at high T, it is hard to extract quantitative information on its resonance energy and intensity.

[40] M. Balkanski, R. F. Wallis, and E. Haro, Phys. Rev. B **28**, 1928 (1983).

[41] N. Taira, M. Wakeshima, and Y. Hinatsu, J. Phys. Condens. Matter **13**, 5527 (2001).

[42] P. Narang, C. A. C. Garcia, and C. Felser, Nat. Mater. **20**, 293 (2021).

[43] S.-Y. Xu *et al.*, Science **332**, 560 (2011).